1	
2	
3	
4	Collision-Induced Unfolding is Sensitive to the
5	Polarity of Proteins and Protein Complexes
6	
7	
8	
9	Seoyeon Hong and Matthew F. Bush*
10	
11	
12	
13	JASMS ASMS-D-19-00130 submitted to J. Am. Soc. Mass Spectrom. on 4/24/2019
14	Revised manuscript submitted on 8/11/2019
15	
16	
17	Contribution from the:
18	University of Washington, Department of Chemistry, Box 351700
19	Seattle, WA 98195-1700
20	
21	*Address correspondence to mattbush@uw.edu
22	

Abstract

23

24

25

26

27

28

29

30

31

32

33

34

35

36

37

38

39

40

Collision-induced unfolding (CIU) uses ion mobility to probe the structures of ions of proteins and noncovalent complexes as a function of the extent of gas-phase activation prior to analysis. CIU can be sensitive to domain structures, isoform identities, and binding partners, which makes it appealing for many applications. Almost all previous applications of CIU have probed cations. Here, we evaluate the application of CIU to anions and compare the results for anions with those for cations. Towards that end, we developed a "similarity score" that we used to quantify the differences between the results of different CIU experiments and evaluate the significance of those differences relative to the variance of the underlying measurements. Many of the differences between anions and cations that were identified can be attributed to the lower absolute charge states of anions. For example, the extents of the increase in collision cross section over the full range of energies depended strongly on absolute charge state. However, over intermediate energies there are significant difference between anions and cations with the same absolute charge state. Therefore, CIU is sensitive to the polarity of protein ions. Based on these results, we propose that the utility of CIU to differentiate similar proteins or noncovalent complexes may also depend on polarity. More generally, these results indicate the relationship between the structures and dynamics of native-like cations and anions deserve further attention and that future studies may benefit from integrating results from ions of both polarities.

Introduction

41

42

43

44

45

46

47

48

49

50

51

52

53

54

55

56

57

58

59

60

61

62

63

In native mass spectrometry (MS), native-like ions are generated using electrospray ionization of proteins, nucleic acids, lipids, and/or other biological molecules in aqueous solutions. Native-like ions can retain noncovalent interactions that were present in solution and therefore native MS can probe the oligomeric state ¹, topology ², and stability ³ of biomolecular complexes in solution. This information can be particularly valuable when the biomolecular complex is too large or small, heterogeneous, or dynamic for other structural tools such as nuclear magnetic resonance, X-ray crystallography, and cryo electron microscopy. For example, native MS of hepatitis B virus capsid proteins provides evidence for complete capsids containing 180 and 240 subunits ⁴, consistent with high-resolution characterization, as well as the stoichiometry of antigen-binding domain binding ⁵ and mechanisms of the assembly process ^{6,7}, which would have been challenging to investigate using conventional techniques. Most native MS experiments have probed native-like cations, although some properties of native-like anions have been investigated ^{8–11}. Typically, native-like anions have lower absolute charge states than the corresponding cations generated from the same solutions ^{9,10}. This systematic difference has been attributed to different extents of charge-carrier emission during the final stages of desolvation ¹⁰, with lower emission energies and therefore greater numbers of competitive emission events ¹² for anions. An atomic-level understanding of the structural differences between cations and anions remains elusive. One obvious difference is that nativelike anions, [M-nH⁺]ⁿ⁻, are proton deficient, whereas native-like cations, [M+nH⁺]ⁿ⁺, are proton rich. Even though these difference will affect hydrogen bonding, salt bridges, and other noncovalent interactions within the ion 13,14 , the collision cross section (Ω) values determined using ion mobility (IM) MS of native-like ions of medium- to large-mass proteins and protein

complexes appear to depend weakly on charge state ^{10,15} and polarity ¹⁰. This suggests that the structural differences between native-like anions and cations may be modest, highly localized, and/or beyond the resolution of current IM measurements.

64

65

66

67

68

69

70

71

72

73

74

75

76

77

78

79

80

81

82

83

84

85

Collisional activation of native-like ions can result in the loss of nonspecific adducts, changes in conformation, and eventually dissociation ¹⁶. Monitoring changes in conformation (collision-induced unfolding, CIU ¹⁷) and extents of dissociation (collision-induced dissociation, CID) as a function of energy can provide information that is complementary to the associated IM and MS characterization of minimally activated ions. For example, CIU can be sensitive to charge state ^{18–20}, domain structure ²¹, isoform identity ²², and ligand binding ^{23–26}. Consequently, there is great interest in using CIU "fingerprints" to differentiate similar proteins ^{22,24,27,28}, particularly in cases where the associated native MS and native IM-MS data are not sensitive to those difference. For example, native-like cations of IgG subclasses with different disulfide bonding have similar Ω values, but exhibit unique CIU features upon the activation ²². Almost all applications of energy-dependent native MS have probed native-like cations. Based on the similarity of the results from CIU of 21+ and 21- ions of serum amyloid P (SAP) pentamers, Hall and coworkers reported that "the conformation and the gas-phase behavior during collisional activation are the same for SAP pentamer, regardless of whether it has an excess of positive or negative charges" ²⁰. For complexes between cholera toxin B subunit homopentamers and five GM1 pentasaccharide ligands, CID of cations results predominantly in the loss of a protein subunit (without a ligand), whereas CID of anions results predominantly in the loss of a ligand (without a protein) ²⁹. These differences suggest that the CID products are a consequence of polarity-dependent structural changes that occur in the gas phase prior to dissociation ²⁹.

It is challenging to assess the general utility of CIU to differentiate similar proteins or complexes because negative results, *i.e.*, cases where CIU is not sensitive to those differences, are usually not reported. Here, in order to broaden the potential utility of CIU, we demonstrate the application of CIU to anions and compare the results for anions with those for cations. Towards that end, we developed a "similarity score" that we use to quantify the differences between the results of different CIU experiments and evaluate the significance of those differences relative to the variance of the underlying measurements.

Methods and Materials

Sample Preparation

Avidin from egg white (A2667, Invitrogen, Carlsbad, CA) and β-lactoglobulin A from bovine milk (product number L7880, Sigma-Aldrich Co., St. Louis, MO) were each buffer exchanged into aqueous 200 mM ammonium acetate at pH 7.0 using centrifugal concentrators (10 kDa MWCO, Spin-X UF, Corning, Inc.) and a centrifuge operated at 4 °C. For charge-reduction experiments, ions were generated from an aqueous solution containing 50 mM trimethylamine and 200 mM ammonium acetate.

Ion Mobility Mass Spectrometry and Collision-Induced Unfolding

Samples were each loaded into glass capillaries with inner diameters of 0.78 mm that were pulled to approximately 1 to 3 µm on one end using a micropipette puller (P-97, Sutter Instruments, Novato, CA). 10 µM protein sample was loaded onto the glass capillary. Electrical contact with the solution was achieved by inserting a platinum wire electrode into the wide end

of the capillary 30 . To minimize analyte carryover between samples, the electrode was washed with aqueous 25% HCl (v:v) and rinsed with ultrapure (18.2 M Ω) water. Data were acquired using a Waters Synapt G2 HDMS hybrid mass spectrometer (Waters Co., Wilmslow, UK) 31 in which the traveling-wave IM cell was replaced with a radio-frequency (RF) confining drift cell 32 that contained 1.7 Torr He. To preserve the noncovalent interactions, the following instrument parameters were used: capillary voltage, ~ 1.0 kV; sampling cone, 20 V; extraction cone, 5 V; source temperature, ~ 30 $^{\circ}$ C; and trap collision energy, 4 V. To determine the mobilities of minimally activated ions, those ions were introduced into the RF-confining drift cell that was operated using at least 9 drift voltages ranging from 104 to 354 V 32 . Ω values of minimally activated ions and the mobility-independent transport times of ions (t_0) were determined from the slopes of plots of drift time versus reciprocal drift voltage as described previously 32 . For CIU experiments, ions were accelerated prior to entering the trap cell using a range of trap injection voltages from 4 to 61 V with the RF confining drift cell operated at a drift voltage of 104 V.

Data Analysis

Mass spectra were analyzed using MassLynx v4.1 (Waters, Co., Milford, MA). Arrival-time distributions were extracted and analyzed using in-house software 33 . The intensities of each arrival-time distribution were normalized so that their sum equals one. To aid in the comparison of IM data, arrival-time distributions were converted to apparent Ω distributions and then interpolated along a common Ω axis. The axes used for avidin and β -lactoglobulin contained 1000 and 500 points, respectively.

Results

Effects of Polarity on the Mass Spectra and Ion Mobility of Native-Like Ions

Figure 1a shows a representative native mass spectrum of avidin that was measured while operating the instrument in positive ion mode and exhibits peaks that are assigned to the 17+, 16+, 15+, and 14+ tetramers of avidin. This spectrum and these assignments are consistent with many examples in the literatures ^{10,34}. Figure 1b shows the analogous spectrum obtained in negative ion mode, which exhibits peaks that are assigned to the 14–, 13–, and 12– tetramers of avidin. The difference in the absolute charge states observed for the two polarities is similar to that reported previously ¹⁰. However, we are not aware of any other reports of native-like anions of avidin in the literature that could be used for comparison. The relative lack of analogous spectra of anions can partially be attributed to the propensity of corona discharge at the tip of electrospray emitters in negative ion mode ³⁵. However, corona discharge was rare in the present experiments, which may be attributable to the low onset voltage for electrospray in this implementation ³⁰.

The native-like cations and anions of avidin were also analyzed using IM-MS, which revealed that the median Ω ($\widetilde{\Omega}$) values of these ions are all similar to each other (Table S1, determined from cumulative distribution function of each apparent Ω distribution as shown in Figure S1). These results corroborate previous results suggesting that gas-phase structure can depend weakly on charge and polarity under native-like conditions 10,20 . However, similar Ω values for native-like cations and anions does not preclude possible differences of anions and cations that are not resolved in these IM measurements. To investigate the potential differences between the cations and anions, we subjected avidin ions to CIU.

Effects of Polarity on the Collision-Induced Unfolding of Native-Like Ions

Selected charge states of native-like cations and anions of avidin were subjected to CIU by varying their laboratory-frame kinetic energy as they enter the trap cell that is positioned immediately prior to the IM cell. Laboratory-frame energy is the product of the voltage used to inject ions in the trap cell and the absolute value of charge state of the ion 36 . The resulting products were then separated by IM and the resulting apparent Ω distributions are shown in Figure 2. The initial distributions are similar for all charge states, consistent with the $\widetilde{\Omega}$ values discussed above. With increasing energy, features appear that are attributed to partially unfolded and mostly unfolded structures, consistent with a previous study of native-like cations of avidin 34 . Although features for folded, partially unfolded, and mostly unfolded avidin ions are observed in all cases, the appearance energy and Ω of these features appear to depend on charge state and polarity to varying extents. Differences are most apparent for the partially unfolded ions. Aspects of these differences will be quantified and discussed in more detail below.

Even though the Ω distributions at low energies are similar for charge states characterized in both polarities, the distributions formed at the highest energies appears to exhibit decreasing magnitudes with decreasing absolute charge state (Figure 2). Figure 3 shows the $\widetilde{\Omega}$ values at the highest (Figure S2) and lowest (Figure S1) energies for each species. The $\widetilde{\Omega}$ values at high energy increase with absolute charge states, which is consistent with visual inspection of the CIU data (Figure 2). The $\widetilde{\Omega}$ value at high energy for the 14– ions is slightly greater than that for the 14+ ions. Because these are the only ions with the same absolute charge state that are observed in both polarities, it is challenging to draw more general conclusions about the effects of polarity on the maximum expansion of protein ions by CIU. In order to further investigate the effects of polarity separately from charge state, trimethylamine was added to an avidin sample,

which was then analyzed in positive ion mode. In these experiments, trimethylamine acts as a charge-reducing agent 37 and enables the formation of 13+ avidin ions. Interestingly, $\tilde{\Omega}$ value at high energy for the 13– ions is less than that for the 13+ ions. However, the binding of trimethylamine is evidenced by the mass spectra shown in <u>Figure S3</u>; the centroids of the peaks in the originating from the sample with trimethylamine correspond to masses that are ~556 Da heavier (equivalent to nearly 10 molecules of trimethylamine) than those originating from the sample without trimethylamine. Based on these results alone, we are unable to conclude whether the differences are a consequence of polarity or the presence of trimethylamine in the sample used to generate the cations. Therefore, this topic will require further investigation in the future.

Although the differences between the $\widetilde{\Omega}$ values at high energies 14+ and 14– are subtle, the CIU results for these ions appear to exhibit more significant differences over intermediate energies (Figures 2b and 2d). For comparison, the apparent Ω distributions for these ions at selected energies are shown in Figure S4. To highlight the differences between the CIU results for these ions of opposing polarity, the difference between those results is plotted in Figure 4a. For comparison, Figures 4b and 4c shows the difference between the Ω distribution of two independent replicates of 14+ and 14– ions, respectively. Although the magnitudes of the differences between replicate analyses of ions of the same polarity (Figures 4b and 4c) are less than the differences between analyses of ions of different polarity (Figure 4a), it was challenging to interpret these differences using these plots alone. For example, the differences at low energies appear as red and blue streaks, but it appears that those differences are the consequence of very slight differences in underlying distributions (e.g., Figure S4a) and that the distributions may have been undersampled in the original experiments. However, both the difference plot (Figure

4a) and the individual Ω distributions (Figure S4) indicate that the greatest differences occur over intermediate energies, in the region associated with partially unfolded structures.

In order to quantitatively compare the apparent Ω distributions underlying these CIU results, we developed a similarity score that depends on the dot products of the pair of distributions and the dot products of duplicate distributions. The similarity score of the distributions for ions α and β is defined as:

Similarity Score =
$$\frac{1}{2} \left(\frac{I_{\alpha} \cdot I_{\beta}}{I_{\alpha} \cdot I_{\alpha}} + \frac{I_{\alpha} \cdot I_{\beta}}{I_{\beta} \cdot I_{\beta}} \right)$$
 (Equation 1)

where I_{α} and I_{β} are the intensities of the distribution for α and β , respectively. Possible scores range between zero and one. A similarity score of one indicates that the two distributions are identical. Conversely, differences in the two distributions will result in similarity scores that are less than one. Figure 4d shows the similarity scores as a function of laboratory frame energy determined from CIU analysis of 14+ and 14- avidin ions, *i.e.*, where α and β have different polarities. This trace is near one for energies <600 eV and near 950 eV, but decreases to significantly lower values near 840 and 1050 eV. Figures S4a to S4e show representative apparent Ω distributions of 14+ and 14- avidin ions at 56, 840, 924, 1036, and 1288 eV. Visual inspection of the distributions at each energy provides context for interpreting the scores determined using Equation 1 and corroborates the preceding evaluation of similarity/difference based only on similarity scores. The results demonstrate the utility of this score for quantifying the similarity between two distributions and identifying the laboratory frame energies that yield the greatest differences for samples from different classes.

Figures 4e and 4f plot the similarity score traces determined for the same data used for the analysis in Figures 4b and 4c, respectively. These traces illustrate typical similarity scores for comparisons between members of the same class. Relative to the traces determined when α and β

have the opposite polarity, these traces are largely independent of energy. To provide context for this data and illustrate sources of variance, Figures S5 and S6 show apparent Ω distributions and similarity scores at selected energies for two pairs of technical replicates. Figure S5 shows that the results for a pair of technical replicates selected for the anions have similarity scores that range from 0.97 to 0.99. At intermediate energies, it appears that a slightly greater fraction of the ions in one replicate have unfolded than in the other, but the differences between the two replicates are very subtle. Figure S6 shows that the results for a pair of technical replicates selected for the cations have similarity scores that range from 0.96 to 0.99. Those slightly lower values appear to be a consequence of a systematic \sim 1 nm² difference in Ω between the two replicates, which were acquired four months apart. Systematic differences could be reduced by acquiring data for different samples on the same day or by standardizing the mobility data 33 .

Figure 5 show similarity score traces that were determined for many independent CIU analyses of 14+ and 14- ions. These results clearly show that the differences between the CIU results for ions of different polarities are significantly greater than the differences between technical replicates for ions of the same polarity. That is, even though the $\tilde{\Omega}$ values at the lowest and the highest energies depend subtly on polarity, the Ω values of the ions generated at intermediate energies depend strongly on polarity. An alternative method for analyzing these results is CIU Suite 2 38 . For example, Figure S7 shows the comparison plot and RMSD values generated using that method, default settings, and the same experimental data used for Figure 4. The RMSD value for ions of different polarity (25%, Figure S7A) is larger than those for ions of the same polarity (10%, Figures S7B and S7C). By comparison, the similarity scores in Figure 5 (1) exhibit far larger differences between ions of different polarity and ions of the same polarity

and (2) directly indicate the energies that are most useful for differentiating between species of interest.

245

246

247

248

249

250

251

252

253

254

255

256

257

258

259

260

261

262

263

264

265

266

In order to evaluate whether other proteins also exhibit polarity-dependent differences, CIU was used to characterize monomers of β-lactoglobulin, which has a mass of 18.4 kDa. Figure S8 shows the native mass spectra of the 7+ and 7- ions, and that features for unadducted protein ions (i.e., no nonspecific adducts) are resolved in both polarities. Unadducted forms of these ions were each quadrupole selected (Figure S8) and subjected to CIU. Unadducted ions are preferred for these experiments because previous studies have shown that that ions subjected to CIU can be stabilized through interactions with nonspecific adducts ^{34,39,40}; unfortunately this was not possible in the preceding example due to presence of multiple glycoforms of avidin 41 and other challenges associated with native MS of higher mass proteins, including decreased apparent resolving power associated with broader isotope distributions ⁴², increased binding of nonspecific adducts ⁴³, and increased scattering with background gas during time-of-flight mass analysis. Figure S9a shows the apparent Ω distributions of 7+ and 7- ions as a function of laboratory frame energy, which reveals very different CIU fingerprints. For example, at 518 eV the 7- anions exhibit a bimodal Ω distribution that is significantly broader than that for the 7+ cations (Figure S4f). The similarity scores are plotted in Figure S9b and indicate that the differences between the results for the anions and cations increase with increasing laboratory frame energy. These results for β-lactoglobulin complement those for avidin and provide further support that the CIU of native-like ions can depend on polarity.

Effects of Polarity on CID Efficiency

The highest energies used for CIU of the avidin tetramer also resulted in CID, yielding monomers and trimers of avidin (Figure S10). The Figure 6a shows the survival yield of quadrupole-selected tetramers ions:

271
$$Survival\ Yield = \frac{\sum I(tetramers)}{\sum I(monomers) + \sum I(trimers) + \sum I(tetramers)}$$
(Equation 2)

The survival yield of the tetramer decreases with increasing laboratory frame energy as a consequence of the formation of monomers and trimers (Figure S10). Activation of the precursor ions also results in the appearance of charge-reduced and higher-charge ions (Figure S11 and S12); such charge-transfer products have been reported previously ⁴⁴. In general, anions exhibit greater propensity for charge stripping than the corresponding cations (Figure S13). Note that survival yields were calculated using all ions observed for each oligomeric state, including any charge-transfer products.

To help compare the stability of each precursor during CID, we determined "LFE₅₀" values, which are defined as the laboratory frame energy that results in a survival yield of 50%. These values for all charge states and both polarities are plotted in Figure 6b. Note that in some cases charge-stripped tetramers may have the same m/z as some trimers. The likelihood of this occurring is greatest for the anions, which exhibit the greatest extent of charge stripping. In order to estimate the possible contributions from such interferences, we calculated LFE₅₀ values for the 13– and 14– ions assuming that the ambiguous ions are entirely trimers (the lower limit) or charge-stripped tetramers (the upper limit). The lower and upper limits of the LFE₅₀ for 14– avidin are 1077 and 1089 eV, respectively. Those limits for 13– avidin are 1141 and 1191 eV, respectively. Since these ranges are small, we did not evaluate this possibility further and use the upper limits in the following discussion.

Overall, the CID efficiency for the native-like anions is less than that of the native-like cations, which to some extent is a consequence of the lower absolute charge states for the former. Figure 6b shows that the LFE₅₀ of 14– avidin is higher than that of the 14+ avidin by 43 eV. 14+ and 14– avidin possess the same charge state but may differ in the presence of mobile protons or charge carriers. For context, numerous studies have concluded that CID of multiprotein complexes involves charge migration to one of the protein subunits, which leads to unfolding and the subsequent ejection of that subunit ^{20,45–49}. Therefore, it is possible that less efficient charge migration in anions, which are proton deficient, may also contribute to their lower CID efficiency. There may be additional consequences of the number of protons in these ions and the concomitant differences in the number of hydrogen bonds and salt bridges ¹³ present in their structures.

Conclusions

Native-like anions and cations of the avidin tetramer were probed using IM-MS, CIU, and CID. Visual inspection of the CIU data for avidin (Figure 2) indicate that there are differences between the results for anions and cations. To analyze the significance of those differences, we developed a "similarity score" (Equation 1) that we used to quantify the differences between results for ions of difference polarities relative to the differences between results for technical replicates of the same polarity (Figure 5). Many of the differences between anions and cations that were identified can be attributed to the lower absolute charge states of anions (Figure 1). For example, the extents of increase in $\widetilde{\Omega}$ values over the full range of energies depended strongly on absolute charge state (Figure 3). However, over intermediate energies there are significant difference between anions and cations with the same absolute charge state

(Figures 4, 5, and S4). Differences between the CIU of anions and cations of β-lactoglobulin were also observed and characterized (Figure S9). These results all indicate that CIU is sensitive to the polarity of protein ions. The CID efficiency of avidin ions also appears to depend on polarity (Figure 6). Characterizing the differences between these properties for additional multiprotein complexes may enable more general insights into the role of charge mobility on dissociation of multiprotein complexes.

Very few native IM-MS experiments have probed anions. Based on results for a selected set of proteins and protein complexes, we reported previously that native-like cations and anions (with minimal activation) can have very similar Ω values and suggested that there was "no inherent benefit to selecting a specific polarity for capturing a more native-like structure" ¹⁰. Because the present results indicate that the CIU of equally charged ions is sensitive to polarity, we propose that the utility of CIU to differentiate similar proteins or noncovalent complexes may depend on polarity. Therefore, we recommend that analyte polarity should be considered during the development of native IM-MS methods for specific applications. More generally, these results indicate the relationship between the structures and dynamics of native-like cations and anions deserve further attention and that future studies may benefit from integrating results from ions of both polarities.

Acknowledgements

This material is based upon work supported by the National Science Foundation under CHE-1807382 (M. F. B.).

Electronic Supplementary Material

336

339

The online version of this article contains supplementary material, which is available to authorized users.

340 References

- 341 (1) Stengel, F.; Baldwin, A. J.; Bush, M. F.; Hilton, G. R.; Lioe, H.; Basha, E.; Jaya, N.;
 342 Vierling, E.; Benesch, J. L. P. Dissecting Heterogeneous Molecular Chaperone Complexes
 343 Using a Mass Spectrum Deconvolution Approach. *Chem. Biol.* **2012**, *19* (5), 599–607.
 344 https://doi.org/10.1016/j.chembiol.2012.04.007.
- Heck, A. J. R. Native Mass Spectrometry: A Bridge between Interactomics and Structural Biology. *Nat. Methods* **2008**, *5* (11), 927–933. https://doi.org/10.1038/nmeth.1265.
- 347 (3) El-Hawiet, A.; Kitova, E. N.; Arutyunov, D.; Simpson, D. J.; Szymanski, C. M.; Klassen, J. S. Quantifying Ligand Binding to Large Protein Complexes Using Electrospray Ionization Mass Spectrometry. *Anal. Chem.* **2012**, *84* (9), 3867–3870. https://doi.org/10.1021/ac3005082.
- Uetrecht, C.; Versluis, C.; Watts, N. R.; Roos, W. H.; Wuite, G. J. L.; Wingfield, P. T.;
 Steven, A. C.; Heck, A. J. R. High-Resolution Mass Spectrometry of Viral Assemblies:
 Molecular Composition and Stability of Dimorphic Hepatitis B Virus Capsids. *Proc. Natl. Acad. Sci.* 2008, 105 (27), 9216–9220. https://doi.org/10.1073/pnas.0800406105.
- 355 (5) Bereszczak, J. Z.; Havlik, M.; Weiss, V. U.; Marchetti-Deschmann, M.; van Duijn, E.;
 356 Watts, N. R.; Wingfield, P. T.; Allmaier, G.; Steven, A. C.; Heck, A. J. R. Sizing up Large
 357 Protein Complexes by Electrospray Ionisation-Based Electrophoretic Mobility and Native
 358 Mass Spectrometry: Morphology Selective Binding of Fabs to Hepatitis B Virus Capsids.
 359 Anal. Bioanal. Chem. 2014, 406 (5), 1437–1446. https://doi.org/10.1007/s00216-013360 7548-z.
- Uetrecht, C.; Barbu, I. M.; Shoemaker, G. K.; van Duijn, E.; Heck, A. J. R. Interrogating
 Viral Capsid Assembly with Ion Mobility–Mass Spectrometry. *Nat. Chem.* 2010, 3, 126.
 https://doi.org/10.1038/nchem.947.
- Lutomski, C. A.; Lyktey, N. A.; Zhao, Z.; Pierson, E. E.; Zlotnick, A.; Jarrold, M. F.
 Hepatitis B Virus Capsid Completion Occurs through Error Correction. J. Am. Chem. Soc.
 2017, 139 (46), 16932–16938. https://doi.org/10.1021/jacs.7b09932.
- Konermann, L.; Douglas, D. J. Unfolding of Proteins Monitored by Electrospray
 Ionization Mass Spectrometry: A Comparison of Positive and Negative Ion Modes. *J. Am. Soc. Mass Spectrom.* 1998, 9 (12), 1248–1254. https://doi.org/10.1016/S1044-0305(98)00103-2.
- Heck, A. J. R.; Heuvel, R. H. H. van den. Investigation of Intact Protein Complexes by
 Mass Spectrometry. *Mass Spectrom. Rev.* 2004, 23 (5), 368–389.
 https://doi.org/10.1002/mas.10081.
- 374 (10) Allen, S. J.; Schwartz, A. M.; Bush, M. F. Effects of Polarity on the Structures and Charge 375 States of Native-Like Proteins and Protein Complexes in the Gas Phase. *Anal. Chem.* 376 **2013**, 85 (24), 12055–12061. https://doi.org/10.1021/ac403139d.
- Liko, I.; Hopper, J. T. S.; Allison, T. M.; Benesch, J. L. P.; Robinson, C. V. Negative Ions
 Enhance Survival of Membrane Protein Complexes. *J. Am. Soc. Mass Spectrom.* 2016, 27
 (6), 1099–1104. https://doi.org/10.1007/s13361-016-1381-5.
- 380 (12) Hogan, C. J.; Carroll, J. A.; Rohrs, H. W.; Biswas, P.; Gross, M. L. Combined Charged 381 Residue-Field Emission Model of Macromolecular Electrospray Ionization. *Anal. Chem.* 382 **2009**, *81* (1), 369–377. https://doi.org/10.1021/ac8016532.

- 383 (13) Loo, R. R. O.; Loo, J. A. Salt Bridge Rearrangement (SaBRe) Explains the Dissociation 384 Behavior of Noncovalent Complexes. *J. Am. Soc. Mass Spectrom.* **2016**, *27* (6), 975–990. 385 https://doi.org/10.1007/s13361-016-1375-3.
- 386 (14) Konermann, L. Molecular Dynamics Simulations on Gas-Phase Proteins with Mobile 387 Protons: Inclusion of All-Atom Charge Solvation. *J. Phys. Chem. B* **2017**, *121* (34), 8102– 388 8112. https://doi.org/10.1021/acs.jpcb.7b05703.
- 389 (15) Laszlo, K. J.; Bush, M. F. Interpreting the Collision Cross Sections of Native-like Protein 390 Ions: Insights from Cation-to-Anion Proton-Transfer Reactions. *Anal. Chem.* **2017**, *89* 391 (14), 7607–7614. https://doi.org/10.1021/acs.analchem.7b01474.
- 392 (16) Benesch, J. L. P. Collisional Activation of Protein Complexes: Picking up the Pieces. *J. Am. Soc. Mass Spectrom.* **2009**, *20* (3), 341–348. https://doi.org/10.1016/j.jasms.2008.11.014.
- 395 (17) Dixit, S. M.; Polasky, D. A.; Ruotolo, B. T. Collision Induced Unfolding of Isolated 396 Proteins in the Gas Phase: Past, Present, and Future. *Curr. Opin. Chem. Biol.* **2018**, *42*, 397 93–100. https://doi.org/10.1016/j.cbpa.2017.11.010.
- 398 (18) Shelimov, K. B.; Jarrold, M. F. Conformations, Unfolding, and Refolding of
 399 Apomyoglobin in Vacuum: An Activation Barrier for Gas-Phase Protein Folding. *J. Am.*400 *Chem. Soc.* **1997**, *119* (13), 2987–2994. https://doi.org/10.1021/ja962914k.
- 401 (19) Pagel, K.; Hyung, S.-J.; Ruotolo, B. T.; Robinson, C. V. Alternate Dissociation Pathways 402 Identified in Charge-Reduced Protein Complex Ions. *Anal. Chem.* **2010**, *82* (12), 5363– 403 5372. https://doi.org/10.1021/ac101121r.
- 404 (20) Hall, Z.; Politis, A.; Bush, M. F.; Smith, L. J.; Robinson, C. V. Charge-State Dependent 405 Compaction and Dissociation of Protein Complexes: Insights from Ion Mobility and 406 Molecular Dynamics. *J. Am. Chem. Soc.* **2012**, *134* (7), 3429–3438. 407 https://doi.org/10.1021/ja2096859.
- 408 (21) Zhong, Y.; Han, L.; Ruotolo, B. T. Collisional and Coulombic Unfolding of Gas-Phase
 409 Proteins: High Correlation to Their Domain Structures in Solution. *Angew. Chem. Int. Ed.*410 **2014**, *53* (35), 9209–9212. https://doi.org/10.1002/anie.201403784.
- 411 (22) Tian, Y.; Han, L.; Buckner, A. C.; Ruotolo, B. T. Collision Induced Unfolding of Intact
 412 Antibodies: Rapid Characterization of Disulfide Bonding Patterns, Glycosylation, and
 413 Structures. *Anal. Chem.* **2015**, *87* (22), 11509–11515.
 414 https://doi.org/10.1021/acs.analchem.5b03291.
- 415 (23) Hopper, J. T. S.; Oldham, N. J. Collision Induced Unfolding of Protein Ions in the Gas
 416 Phase Studied by Ion Mobility-Mass Spectrometry: The Effect of Ligand Binding on
 417 Conformational Stability. *J. Am. Soc. Mass Spectrom.* 2009, 20 (10), 1851–1858.
 418 https://doi.org/10.1016/j.jasms.2009.06.010.
- 419 (24) Hyung, S.-J.; Robinson, C. V.; Ruotolo, B. T. Gas-Phase Unfolding and Disassembly
 420 Reveals Stability Differences in Ligand-Bound Multiprotein Complexes. *Chem. Biol.* 421 2009, 16 (4), 382–390. https://doi.org/10.1016/j.chembiol.2009.02.008.
- 422 (25) Rabuck, J. N.; Hyung, S.-J.; Ko, K. S.; Fox, C. C.; Soellner, M. B.; Ruotolo, B. T.
 423 Activation State-Selective Kinase Inhibitor Assay Based on Ion Mobility-Mass
 424 Spectrometry. *Anal. Chem.* 2013, 85 (15), 6995–7002. https://doi.org/10.1021/ac4012655.
- Zhao, Y.; Yang, J. Y.; Thieker, D. F.; Xu, Y.; Zong, C.; Boons, G.-J.; Liu, J.; Woods, R.
 J.; Moremen, K. W.; Amster, I. J. A Traveling Wave Ion Mobility Spectrometry (TWIMS)
 Study of the Robo1-Heparan Sulfate Interaction. J. Am. Soc. Mass Spectrom. 2018, 29 (6),
 1153–1165. https://doi.org/10.1007/s13361-018-1903-4.

- 429 (27) Rabuck-Gibbons, J. N.; Lodge, J. M.; Mapp, A. K.; Ruotolo, B. T. Collision-Induced 430 Unfolding Reveals Unique Fingerprints for Remote Protein Interaction Sites in the KIX 431 Regulation Domain. *J. Am. Soc. Mass Spectrom.* **2018**. https://doi.org/10.1007/s13361-432 018-2043-6.
- 433 (28) Wagner, N. D.; Clemmer, D. E.; Russell, D. H. ESI-IM-MS and Collision-Induced
 434 Unfolding That Provide Insight into the Linkage-Dependent Interfacial Interactions of
 435 Covalently Linked Diubiquitin. *Anal. Chem.* **2017**, *89* (18), 10094–10103.
 436 https://doi.org/10.1021/acs.analchem.7b02932.
- 437 (29) Zhang, Y.; Deng, L.; Kitova, E. N.; Klassen, J. S. Dissociation of Multisubunit Protein– 438 Ligand Complexes in the Gas Phase. Evidence for Ligand Migration. *J. Am. Soc. Mass* 439 *Spectrom.* **2013**, *24* (10), 1573–1583. https://doi.org/10.1007/s13361-013-0712-z.
- 440 (30) Davidson, K. L.; Oberreit, D. R.; Hogan, C. J.; Bush, M. F. Nonspecific Aggregation in 441 Native Electrokinetic Nanoelectrospray Ionization. *Int. J. Mass Spectrom.* **2016**, *420* (8), 442 34–42. https://doi.org/10.1016/j.ijms.2016.09.013.
- 443 (31) Giles, K.; Williams, J. P.; Campuzano, I. Enhancements in Travelling Wave Ion Mobility
 444 Resolution. *Rapid Commun. Mass Spectrom.* **2011**, *25* (11), 1559–1566.
 445 https://doi.org/10.1002/rcm.5013.
- 446 (32) Allen, S. J.; Giles, K.; Gilbert, T.; Bush, M. F. Ion Mobility Mass Spectrometry of 447 Peptide, Protein, and Protein Complex Ions Using a Radio-Frequency Confining Drift 448 Cell. *The Analyst* **2016**, *141* (3), 884–891. https://doi.org/10.1039/c5an02107c.
- 449 (33) Bush, M. F.; Campuzano, I. D. G.; Robinson, C. V. Ion Mobility Mass Spectrometry of 450 Peptide Ions: Effects of Drift Gas and Calibration Strategies. *Anal. Chem.* **2012**, *84* (16), 451 7124–7130. https://doi.org/10.1021/ac3014498.
- 452 (34) Freeke, J.; Bush, M. F.; Robinson, C. V.; Ruotolo, B. T. Gas-Phase Protein Assemblies:
 453 Unfolding Landscapes and Preserving Native-like Structures Using Noncovalent Adducts.
 454 Chem. Phys. Lett. 2012, 524, 1–9. https://doi.org/10.1016/j.cplett.2011.11.014.
- 455 (35) McClory, P. J.; Håkansson, K. Corona Discharge Suppression in Negative Ion Mode 456 Nanoelectrospray Ionization via Trifluoroethanol Addition. *Anal. Chem.* **2017**, *89* (19), 457 10188–10193. https://doi.org/10.1021/acs.analchem.7b01225.
- 458 (36) Laskin, J.; Futrell, J. H. Activation of Large Ions in FT-ICR Mass Spectrometry. *Mass Spectrom. Rev.* **2005**, *24* (2), 135–167. https://doi.org/10.1002/mas.20012.
- 460 (37) Zhuang, X.; Gavriilidou, A. F. M.; Zenobi, R. Influence of Alkylammonium Acetate
 461 Buffers on Protein–Ligand Noncovalent Interactions Using Native Mass Spectrometry. J.
 462 Am. Soc. Mass Spectrom. 2017, 28 (2), 341–346. https://doi.org/10.1007/s13361-016 463 1526-6.
- 464 (38) Polasky, D. A.; Dixit, S. M.; Fantin, S. M.; Ruotolo, B. T. CIUSuite 2: Next-Generation 465 Software for the Analysis of Gas-Phase Protein Unfolding Data. *Anal. Chem.* **2019**, *91* (4), 466 3147–3155. https://doi.org/10.1021/acs.analchem.8b05762.
- 467 (39) Han, L.; Hyung, S.-J.; Mayers, J. J. S.; Ruotolo, B. T. Bound Anions Differentially
 468 Stabilize Multiprotein Complexes in the Absence of Bulk Solvent. *J. Am. Chem. Soc.*469 **2011**, *133* (29), 11358–11367. https://doi.org/10.1021/ja203527a.
- 470 (40) Han, L.; Hyung, S.-J.; Ruotolo, B. T. Bound Cations Significantly Stabilize the Structure 471 of Multiprotein Complexes in the Gas-Phase. *Angew. Chem. Int. Ed Engl.* **2012**, *51* (23), 472 5692–5695. https://doi.org/10.1002/anie.201109127.

- 473 (41) DeLange, R. J.; Huang, T. S. Egg White Avidin. 3. Sequence of the 78-Residue Middle Cyanogen Bromide Peptide. Complete Amino Acid Sequence of the Protein Subunit. *J. Biol. Chem.* **1971**, *246* (3), 698–709.
- 476 (42) Lössl, P.; Snijder, J.; Heck, A. J. R. Boundaries of Mass Resolution in Native Mass
 477 Spectrometry. J. Am. Soc. Mass Spectrom. 2014, 25 (6), 906–917.
 478 https://doi.org/10.1007/s13361-014-0874-3.
- 479 (43) Benesch, J. L. P.; Ruotolo, B. T.; Simmons, D. A.; Robinson, C. V. Protein Complexes in 480 the Gas Phase: Technology for Structural Genomics and Proteomics. *Chem. Rev.* **2007**, 481 107 (8), 3544–3567. https://doi.org/10.1021/cr068289b.
- 482 (44) Sobott, F.; McCammon, M. G.; Robinson, C. V. Gas-Phase Dissociation Pathways of a Tetrameric Protein Complex. *Int. J. Mass Spectrom.* **2003**, *230* (2), 193–200. https://doi.org/10.1016/j.ijms.2003.09.008.
- 485 (45) Felitsyn, N.; Kitova, E. N.; Klassen, J. S. Thermal Decomposition of a Gaseous
 486 Multiprotein Complex Studied by Blackbody Infrared Radiative Dissociation.
 487 Investigating the Origin of the Asymmetric Dissociation Behavior. *Anal. Chem.* 2001, 73
 488 (19), 4647–4661. https://doi.org/10.1021/ac0103975.
- 489 (46) Jurchen, J. C.; Williams, E. R. Origin of Asymmetric Charge Partitioning in the
 490 Dissociation of Gas-Phase Protein Homodimers. *J. Am. Chem. Soc.* **2003**, *125* (9), 2817–
 491 2826. https://doi.org/10.1021/ja0211508.
- 492 (47) Jurchen, J. C.; Garcia, D. E.; Williams, E. R. Further Studies on the Origins of
 493 Asymmetric Charge Partitioning in Protein Homodimers. J. Am. Soc. Mass Spectrom.
 494 2004, 15 (10), 1408–1415. https://doi.org/10.1016/j.jasms.2004.06.006.
- (48) Fegan, S. K.; Thachuk, M. A Charge Moving Algorithm for Molecular Dynamics
 Simulations of Gas-Phase Proteins. J. Chem. Theory Comput. 2013, 9 (6), 2531–2539.
 https://doi.org/10.1021/ct300906a.
- 498 (49) Popa, V.; Trecroce, D. A.; McAllister, R. G.; Konermann, L. Collision-Induced
 499 Dissociation of Electrosprayed Protein Complexes: An All-Atom Molecular Dynamics
 500 Model with Mobile Protons. J. Phys. Chem. B 2016, 120 (23), 5114–5124.
 501 https://doi.org/10.1021/acs.jpcb.6b03035.
 502

(a) 16+ 17+ 15+ 14-12-3500 4000 4500 5000 5500 m/z

Figure 1. Native mass spectra of avidin in positive (a) and negative (b) polarity obtained from an aqueous solution of 200 mM ammonium acetate at pH 7.0. The predominant peaks are assigned to tetramers, with charge states as labeled. The weak signals at higher m/z are assigned to dimers of the avidin tetramer, which is attributed to nonspecific aggregation during electrospray ionization 30 .

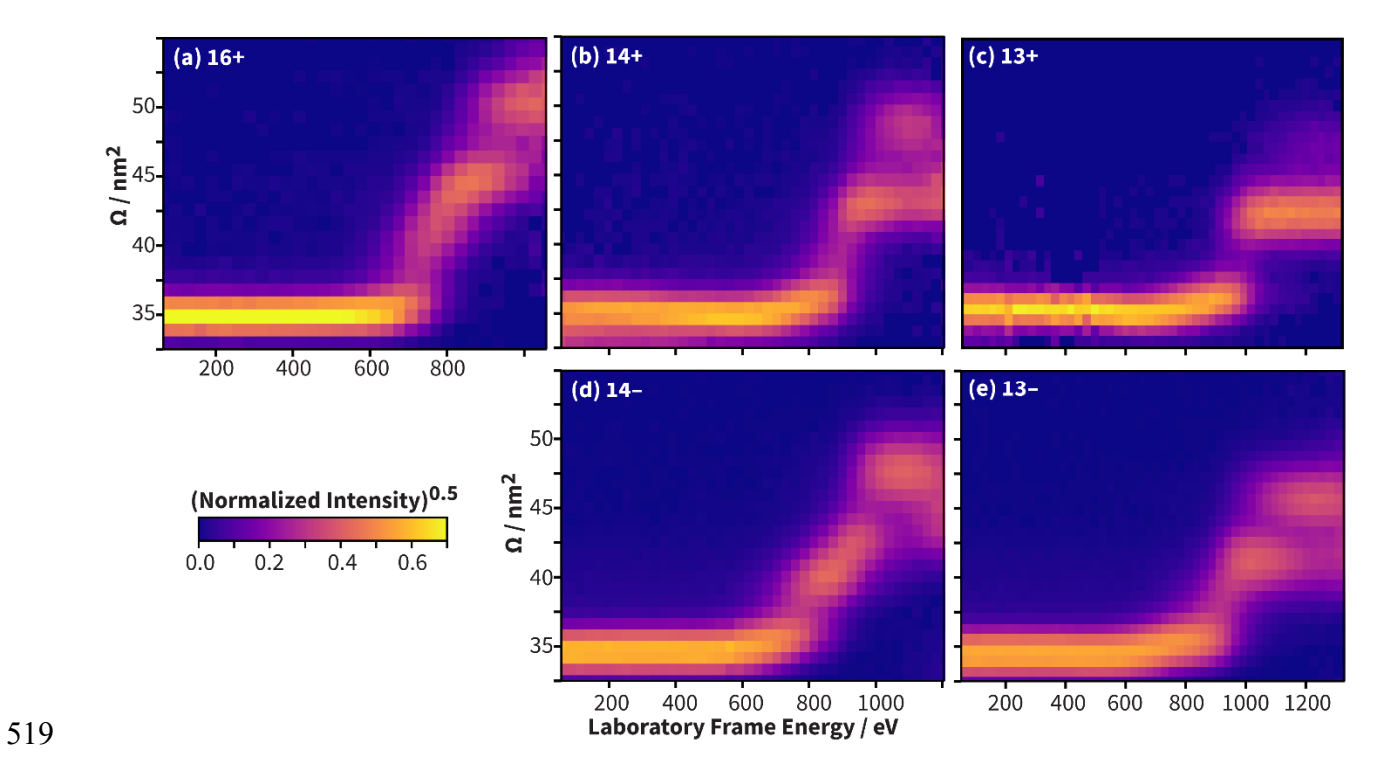


Figure 2. Results from collision-induced unfolding (CIU) of selected charge states of the avidin tetramer. Ions were generated from an aqueous solution containing 200 mM ammonium acetate, except the 13+ ions were generated from a solution that also contained 50 mM trimethylamine. The heat maps display the Ω distributions as a function of laboratory frame energy, based on data acquired using 2 V increments of the trap injection voltage. Laboratory frame energy was increased until the precursor was depleted due to dissociation.

Charge- Anions Cations
Reduced Cations

13

14

Absolute Charge State

Figure 3. The median Ω ($\widetilde{\Omega}$) value at low (20 V) and high (16+: 64 V, 15+: 68 V, 14+: 86 V, 13+: 118 V, 14-:86 V, 13-:100 V) trap injection voltage. Each marker represents the average of the $\widetilde{\Omega}$ values determined for three intendent technical replicates. The vertical bars span the 95% confidence interval of the replicates. The upper and low bound of the shaded region represent the Ω values at 90% and 10% of the cumulative distribution function respectively, as shown in Figures S1 and S2.



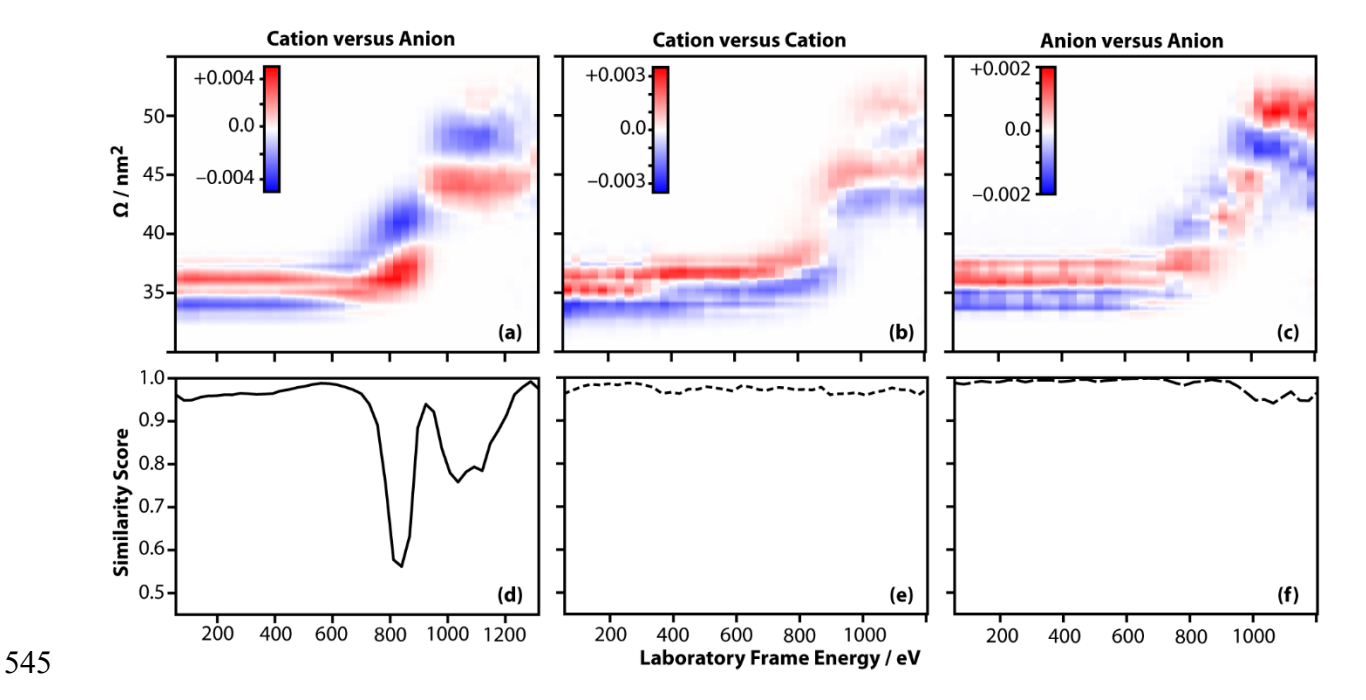


Figure 4. (a) The differences between the CIU intensities for 14+ and 14- avidin from native-like conditions. *Reds* indicate greater relative intensities for the cations (positive values), whereas *blues* indicate greater relative intensities for the anions (negative values). The differences between the CIU intensities based on two independent technical replicates of 14+ and 14- avidin are shown in (b) and (c), respectively. (d) The similarity scores (Equation 1) for the apparent Ω distributions of 14+ and 14- avidin used for (a). The similarity scores for the apparent Ω distributions used for (b) and (c) are plotted in (e) and (f), respectively.

1.0-0.9-0.8-0.6-0.5-200 400 600 800 1000 1200 Laboratory Frame energy / eV

Figure 5. Similarity scores of results for 14+ and 14– avidin ions (*solid lines*) determined from unique pairs of three replicate CIU analyses of 14+ and 14– avidin. Similarity scores for unique pairs of replicate CIU analyses of 14+ (*dotted lines*) and 14– (*dashed lines*) avidin.



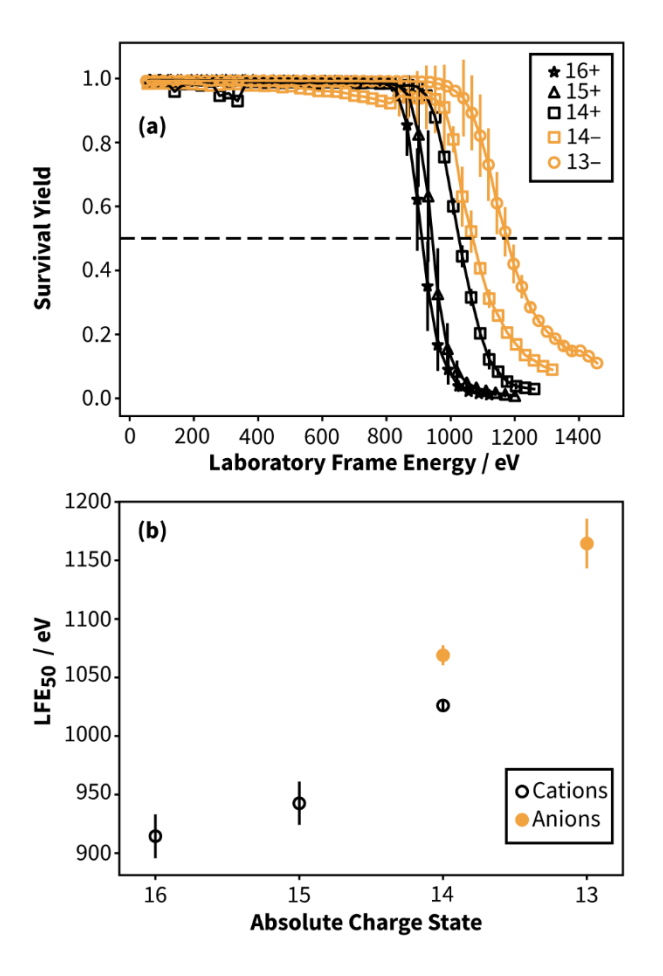


Figure 6. Results from collision-induced dissociation (CID) of avidin ions from native-like conditions. Representative mass spectra are shown in Figure S10. (a) Survival yield of the precursor ions as function of laboratory frame energy. The bars span the 95% confidence interval of three independent technical replicates. Note that replicates were not collected for laboratory frame energies that are far greater or lower than the LFE₅₀. (b) LFE₅₀ for each charge state is shown in both polarities. The bars span the 95% confidence interval based on three independent technical replicates.